Dobrowolska, M., Velthuis, J., Frazao, L., & Kikola, D. (2018). A novel technique for finding gas bubbles in the nuclear waste containers using Muon Scattering Tomography. *Journal of Instrumentation*, *13*(5), [P05015]. https://doi.org/10.1088/1748-0221/13/05/P05015

A novel technique for finding gas bubbles in the nuclear waste containers using Muon Scattering Tomography

M. Dobrowolska [a,1] **J. Velthuis**[b] **L. Frazão**[b] **D. Kikoła**[a]

[a] *Faculty of Physics, Warsaw University of Technology, Koszykowa 75, 00-662 Warsaw, Poland*

[b] *School of Physics, HH Wills Physics Laboratory, University of Bristol, Tyndall Avenue, BS8 1TL, Bristol, United Kingdom.*

E-mail: magdalena.dobrowolska@fizyka.pw.edu.pl

Abstract: Nuclear waste is deposited for many years in the concrete or bitumen-filled containers. With time hydrogen gas is produced, which can accumulate in bubbles. These pockets of gas may result in bitumen overflowing out of the waste containers and could result in spread of radioactivity. Muon Scattering Tomography is a non-invasive scanning method developed to examine the unknown content of nuclear waste drums. Here we present a method which allows us to successfully detect bubbles larger than 2 litres and determine their size with a relative uncertainty resolution of 1.55 ± 0.77%. Furthermore, the method allows to make a distinction between a conglomeration of bubbles and a few smaller gas volumes in different locations.

Keywords: Counting gases and liquids; Models and simulations; Radiation monitoring; Resistive-plate chambers

[1]Corresponding author

Contents

1 Introduction

1.1 Nuclear waste management

Nuclear power plants generate radioactive waste as a result of their activities. The risks associated with such materials are significant. Consequently, safe storage and transportation of those materials are essential. In some countries low and intermediate level nuclear waste is stored in steel containers with either pure bitumen added to fill the free volume, or after mixing of the waste with bitumen [1–3]. In both cases irradiation of the bitumen by the nuclear waste results in the production of hydrogen [4–6]. Since bitumen is impermeable to water and gases, this hydrogen can congregate in bubbles, possibly resulting in bitumen overflowing out of the waste containers. This could result in spread of radioactivity and difficulties with manipulation of the drums. It is therefore important to develop techniques to detect the amount of gas formed in the containers. Furthermore, it is of great interest to determine whether the gas formed is evenly distributed in small bubbles or concentrated in bigger bubbles. As far as we know, no satisfactory solution has been found to determine the volume of gas in such vessels.

Here a method is presented for gas detection in waste containers. We propose a novel technique that employs Muon Scattering Tomography for detection of low-density materials. Muon Scattering Tomography is well known and widely used for many years technique. The technique presented in this publication is based on the approach shown in [7] and further developed to estimating the volume of gas present in nuclear waste containers. It allows to detect and measure the volume of gas bubbles inside the waste drums. We also present an algorithm to determine where bubbles are located including a distinction between a big pocket of gas and a few smaller gas areas. The performance of the proposed method is verified using realistic Monte Carlo simulations of a muon detection system.

1.2 Muon Scattering Tomography

Muon Scattering Tomography is a method developed for the scanning of objects. It uses cosmic muons to determine the contents of a closed volume from a safe distance. The technique has been developed for many different applications [7–21]. The main advantage is its non-invasiveness, no additional radiation is introduced to perform the scan. Furthermore, cosmic radiation is abundant. The cosmic muon flux at sea level is about 10000 $m^{-2}min^{-1}$ [22] and has a wide angular and momentum spread, see Figure 1. Cosmic muons are highly penetrating, so they are perfect in situations where the tested volume is shielded by a layer of metal or rock [21]. Furthermore, since muons are charged particles, they are relatively easy to detect.

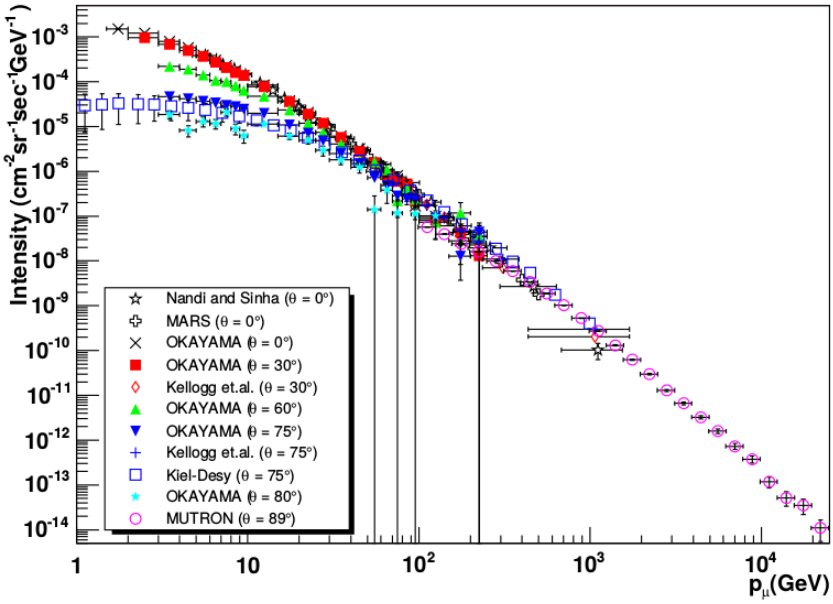

Figure 1: Muon intensity as a function of muon momentum, where θ is the zenith angle [23].

The method is based on measuring the incoming and outgoing tracks of muons, see Figure 2a. Muons undergo multiple scattering in matter. The distribution of the scattering angle can be described by a Gaussian distribution with a mean of zero and standard deviation σ_θ, which depends on the atomic number, Z, of the traversed medium. The standard deviation is given by [24]:

$$\sigma_\theta \approx \frac{13.6MeV}{pc\beta}\sqrt{\frac{T}{X_0}}\,[1 + 0.038\,ln(\frac{T}{X_0})] \tag{1.1}$$

$$X_0 \approx \frac{716.4A}{Z(Z+1)\ln(\frac{287}{\sqrt{Z}})}\ [g \cdot cm^{-2}] \tag{1.2}$$

where p is muon's momentum, β is muon's speed divided by the speed of light c, T is the thickness of the material, X_0 is radiation length of the material. A is the atomic weight of the medium in $g \cdot mol^{-1}$. Here we assume that the tracks share a common point (the vertex), see Figure 2b. Since muons undergo multiple Coulomb scattering in matter, the vertex assumption is not strictly correct.

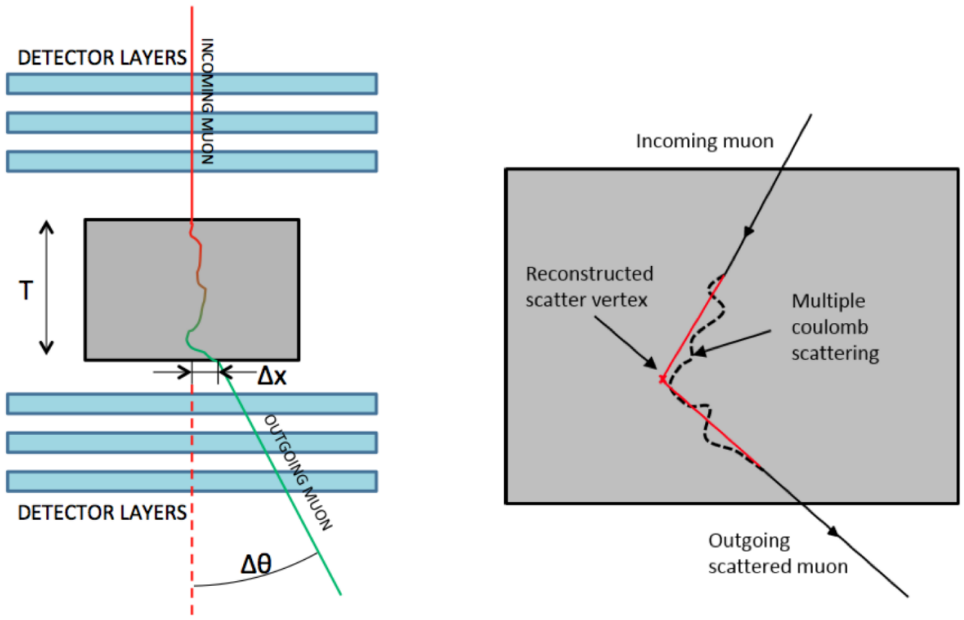

(a) The muon's trajectory is measured before and after traversing the volume under test.

(b) Vertex reconstruction.

Figure 2: Muon Scattering Tomography principle [8].

However, it is a useful approximation, since it nonetheless provides a roughly correct localization of the area of the muon scattering for the larger scattering events used in our method. The methods presented in [8], [10], [21] were developed for detecting and distinguishing small lumps of high-Z materials and measure their size. Here, the method was further developed and used to distinguish low-Z (gas) from a higher-Z (concrete-like) material and measuring the size of gas bubbles.

1.3 Model set up

Each time 159 million muons were simulated. This corresponds to about 16 days of data taking at the sea level, considering the inclusive muon flux. The time of data collection was chosen as a compromise between the measurement time tolerable for application in the industry, and the accuracy of the study (the larger the data sample, the better the resolution of the measured volume). As the term bitumen is not very well defined [25] it was chosen to simulate a concrete-like material with a density of 2.3 g/cm^3. Hydrogen gas bubbles were simulated as a gas with a density of $1.2 \cdot 10^{-3}$ g/cm^3. The analysis presented here is based on simulated data tuned to the performance and design of a prototype system built at the University of Bristol [21], [26].

In this study, a realistic muon sample is generated using the CRY library [27], which is the most reliable tool we found for this purpose. Since this paper presents a proof-of-principle study of the proposed method, the cosmic ray flux at sea level was used although we are aware that high level waste is usually stored underground. Estimation of a muon flux in an underground waste repository requires knowledge about the structure of the repository (depth, etc). Furthermore, the main difference between muons at the surface and underground is the flux. Hence, it will take longer

to get the same number of muons but the results will be the same for the same amount of muons. Moreover, intermediate-level and short-lived low-level radioactive waste are sometimes disposed at ground level.

For this first study, we assume that the experimental system will be able to measure the muon momentum. The momentum value is taken from the simulation by the CRY library and it is not smeared. The passage of the muons through the detectors and volume under test is simulated using GEANT4 [28]. A schematic geometry used in the simulations is presented in Figure 3. Muon Scattering Tomography uses a series of detectors installed on both sides of the object under test, usually above and below [21]. The simulated detector model consists of six pairs of resistive plate chambers (RPCs). Three pairs are located above the examined object (whereby the incoming tracks are reconstructed), three of them are under (from which the reconstruction of the outgoing tracks is carried out). The dimensions of each of the RPCs are 100x100 cm^2, and the thickness is 6 mm. One pair houses both X and Y planes, perpendicular to each other, so they can measure both x and y coordinates. The spacing between each X and Y plane is 19 mm while the gap between each of the pairs is 58 mm. The distance between the upper and the lower RPC pairs is 548 mm. The RPCs strips have a pitch of 1.5 mm [10]. In addition, we defined a cylindrical waste drum with the radius of 13 cm and length of 40 cm, which was placed between the top and bottom half of the detector system. The drum is placed in the center of the system. Its steel outer casing has a thickness of 1.5 cm. The steel base located under the object is 2 cm thick, and on top there is a 3.5 cm thick steel cap. Based on [26] a spatial resolution of 450 μm was chosen for the RPCs. From the reconstructed tracks, variables relating to the scattering behaviour can be calculated.

1.4 Metric method

In this study, the metric method as presented in [7] is used. The basis of the metric method is to divide the volume under investigation into voxels with sides of 10 mm. The method exploits that in dense material high angle scattering takes place more frequently. For that reason, the vertices, present in a given voxel, associated with high angle scattering in high-Z lumps are closer to each other than in low-Z material. Using the vertices assigned to the voxel, the weighted metric value is calculated for each pair of vertices reconstructed in a given cubic bin. The weighted metric, $\widetilde{m_{ij}}$, is the absolute metric distance between each pair of vertices in that cubic bin, normalized by the scattering angle and momentum [8]:

$$\widetilde{m_{ij}} = \frac{\|\boldsymbol{V_i} - \boldsymbol{V_j}\|}{(\theta_i p_i) \cdot (\theta_j p_j)} \tag{1.3}$$

where $\boldsymbol{V_i}$ is the position of the muon i vertex, θ_i is the scatering angle and p_i is the momentum of muon i. Then the median of the weighted metric distribution is determined for each cubic bin. The median is referred to as the discriminator [8]. The distribution of the calculated medians has become the starting point for further work. In low-Z materials high angle scattering occurs less often than in high-Z materials. Therefore in less dense materials vertices are further apart and thus a higher discriminator is found for lower Z materials.

Figure 4 shows the discriminator distributions of a gas-filled drum and a concrete-filled drum. The distributions are clearly distinct. Empty drums (low-Z material inside vessel) can be clearly distinguished from concrete-filled drums (higher-Z material inside vessel) as low-Z material is

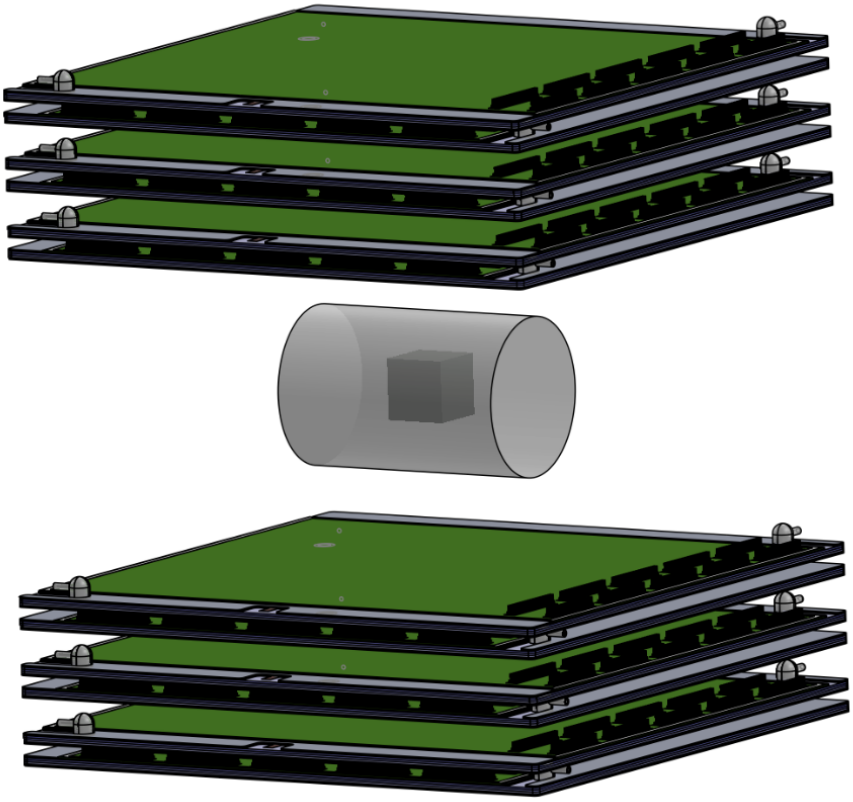

Figure 3: Geometry used in simulations [10]. Each RPC measures 100x100 cm^2. The distance between single X and Y planes is 19 mm while the spacing between each pair of resistive plate chambers is 58 mm. The distance between the upper and the lower RPC pairs is 548 mm.

characterized by higher values of the discriminator. The effective variable for detection of a gas volume V should have a monotonic dependence on V, with the largest possible gradient to maximise the sensitivity. We tested different variables. The studies showed that the mean of the distribution of the discriminator, μ_{discr}, gives the best information about the amount of gas in the examined tube. The mean, μ_{discr}, for the empty drum is 10.244 ± 0.003 and for the concrete-filled drum is 10.069 ± 0.003.

2 Results

First we will demonstrate the effectiveness of the algorithm to find bubbles of gas in the concrete. Then we will demonstrate that this is only dependent on the volume of the bubbles and not on the shape or location. Finally, we will show that it is possible to locate the bubbles and see the difference between one large and two smaller bubbles.

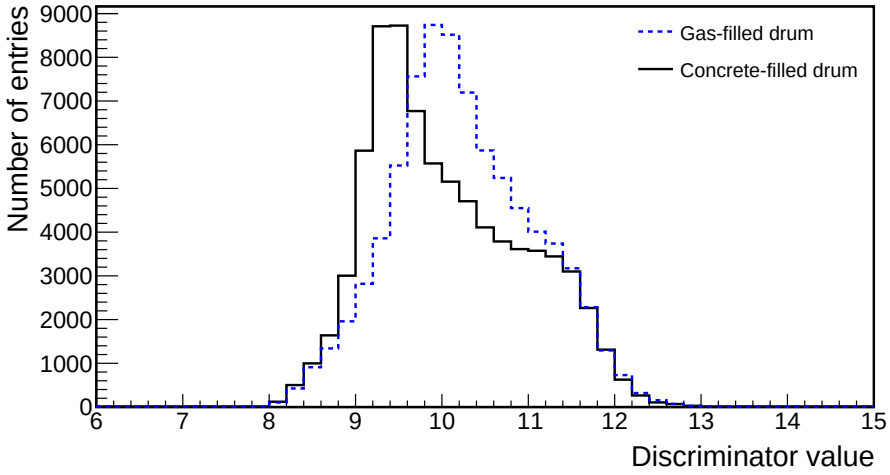

Figure 4: The discriminator distribution for the gas-filled drum (blue dotted line) and concrete-filled drum (solid black line).

radius [cm]	lenght [cm]	volume of gas [cm^3]
2	4	50.27
2	5	62.83
2	6	75.40
3	9	254.47
4	10	502.65
5	15	1178.10
7	13	2001.19
7	19	2924.82
8	22	4423.36
8	30	6031.86
9	28	7125.13
10	30	9424.78
11	34	12924.51
12	38	17190.80
13	40	21237.17

Table 1: Dimensions of gas bubbles in the simulations.

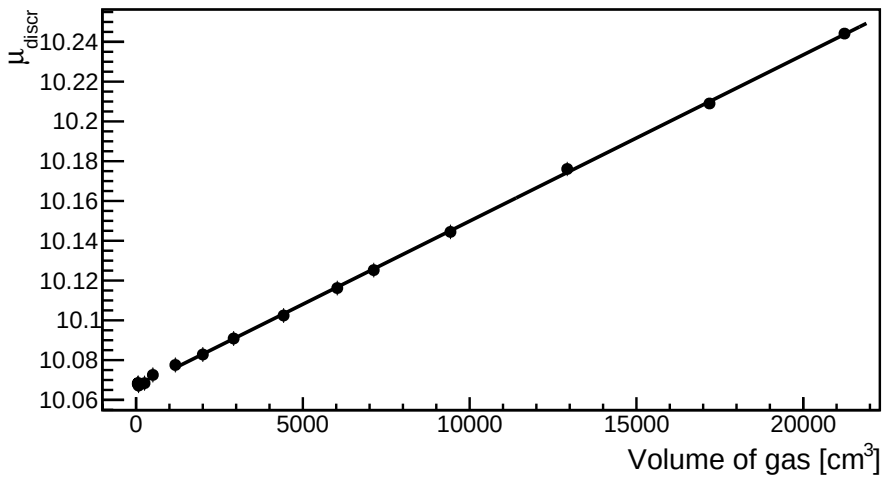

Figure 5: The mean of the discriminator distribution, μ_{discr}, as a function of the real volume of gas in concrete-filled drum.

2.1 Identification of the gas volume in a container

Simulations, introducing different sizes of gas bubbles inside the concrete-filled drum, were performed. Bubbles were cylindrical in shape with various radius, lengths, see Table 1, and they were placed in the center of the drum. For each configuration the mean, μ_{discr}, of the discriminator distribution was calculated and plotted. As can be seen in Figure 5, μ_{discr} is an excellent measure of the total amount of gas V. It provides a linear dependence of the μ_{discr} on the amount of gas. A fit starting from 1 litres shows that μ_{discr} as a function of gas volume V is well described by the equation:

$$\mu_{discr} = (8.36 \pm 0.15) \times 10^{-6} V + (10.066 \pm 0.002) \tag{2.1}$$

The formula 2.1 describes a general relation of a gas volume and the mean of the discriminator distribution, it takes into account all simulated geometries described in Table 1 larger than 1 litre.

To reconstruct a given volume, the straight line was fitted to all points except the one being reconstructed. Next, the gas volume V_{reco} for the omitted point is calculated based on inverting the formula obtained from the fit to all points except the one being reconstructed. This procedure is repeated for all volumes in Table 1. Figure 6 shows the reconstructed volume V_{reco} as a function of the actual one V. There is a very clear straight line dependence between the reconstructed V_{reco} and actual volume V. Figure 7 shows the relative uncertainty of the reconstructed volume V_{reco} as a function of the real gas volume V for volumes larger than 1 litre. The result shows that we are able to detect volume of gas of about 1 litre with a relative uncertainty of the reconstructed volume around of 19%. The relative uncertainty of the reconstructed volume for larger volumes is much smaller. Figure 8 shows the distribution of the relative uncertainty of the reconstructed volume for volumes larger than 1 litre. The obtained relative uncertainty resolution of the reconstructed volume is 1.55 ± 0.77%. The outlier at −18 refers to geometry simulated with a 1.2 litres bubble inside. This result

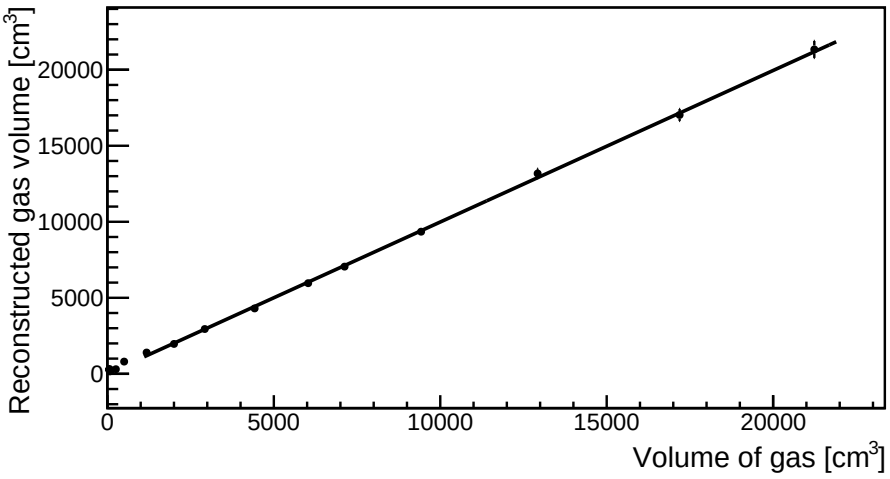

Figure 6: The reconstructed volume of gas as a function of the real volume of gas in concrete-filled drum.

demonstrates that bubbles with a volume exceeding 2 litres can be detected and their size measured with high precision.

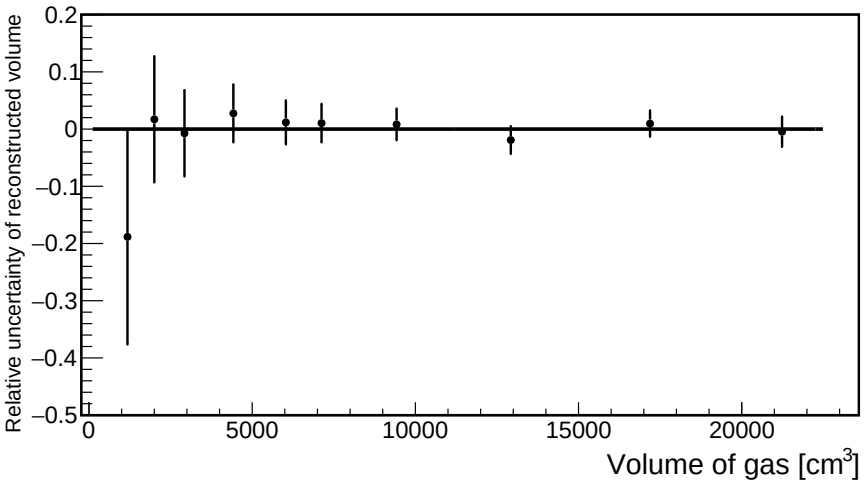

Figure 7: The relative uncertainty of the reconstructed volume as a function of the real volume of gas in concrete-filled drum for volumes larger than 1 litre.

2.2 The sensitivity of the method for bubbles of various shapes, sizes and locations

In the result presented in section 2.1, the bubbles were cylindrical and placed in the center of the drum. If the shape or location would influence the result, the method would be of limited use. In this section, cylindrical bubbles were compared to spherical bubbles that were also placed in the centre of the drum. Next, cylindrical bubbles were compared to spherical bubbles that were shifted away from the centre. Finally, the total volume of the bubbles was split into two equal size bubbles of half

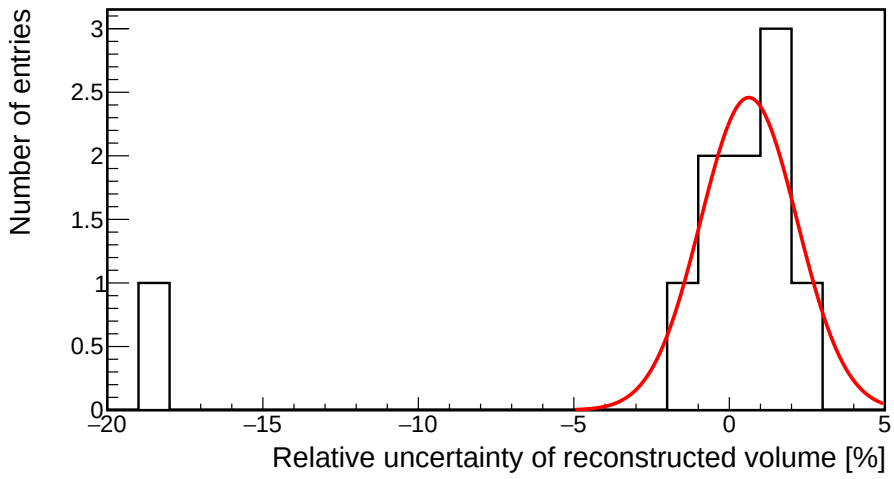

Figure 8: Distribution of the relative uncertainty of the reconstructed volume for volumes larger than 1 litre.

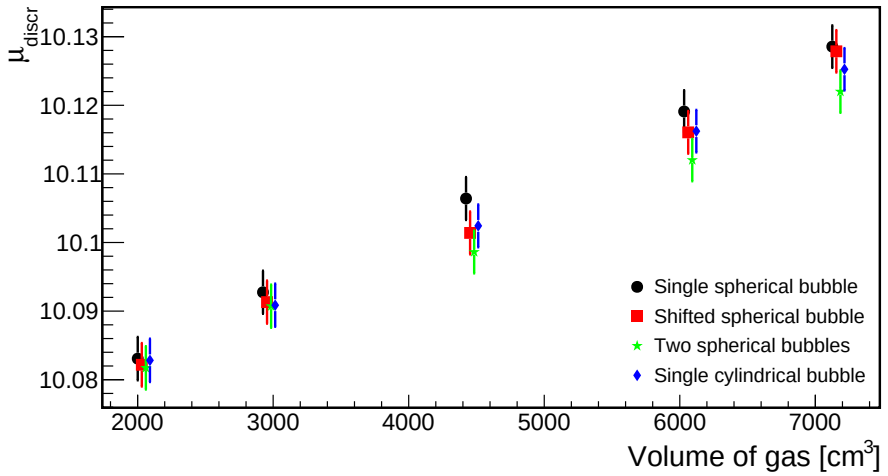

Figure 9: Mean of the discriminator distribution as a function of the real volume of gas in concrete-filled drum for different geometries of bubbles. In order to make the results visible, a small horizontal offset was applied to each data set. The actual volume of gas is the one for the single spherical bubble series.

the original volume and compared with cylindrical bubbles. The results of this study are presented in Figure 9. The result shows that the same μ_{discr} is obtained within errors for the same volume for all four cases. Hence, based on the cases considered, the method is insensitive to the location and shape of the bubble. This makes the method applicable in reality as the key task is detecting and measuring the overall size of gas bubbles.

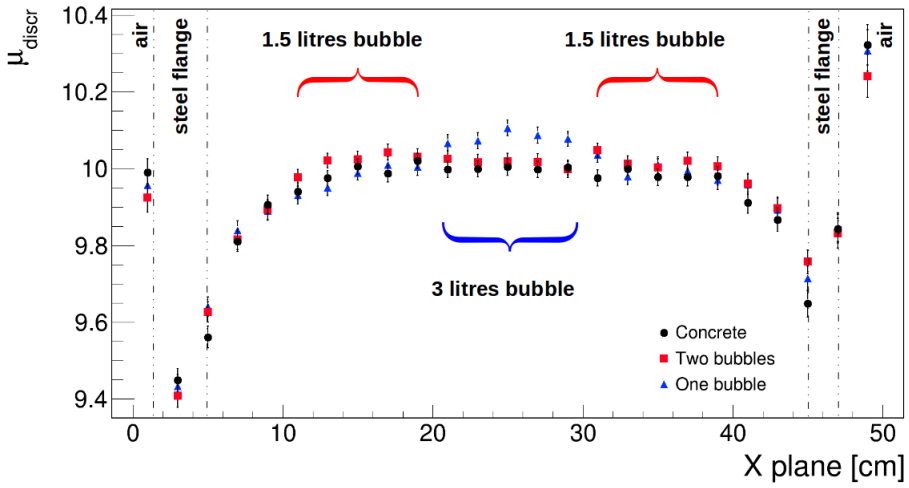

Figure 10: The concrete-filled drum with 3 litres bubble inside (blue triangles) or two 1.5 litres bubbles (red squares).

2.3 Determining the location of gas volumes

In the previous section, it was demonstrated that the method is not sensitive to the location or shape of the bubble. However, the location of bubbles can be determined if the analysis is applied to individual slices of the drum. This also allows to discriminate between single big bubbles and a set of smaller bubbles. The examinated drum was divided into slices along x-axis. The x-axis is chosen to coincide with the central axis of the cylinder. Each slice was 2 cm in length. For every section the mean value of discriminator distribution, μ_{discr}, was calculated. Figure 10 and 11 show the μ_{discr} as a funcion of x-slice, for three different geometries: a concrete-filled drum, a concrete-filled drum with one bubble and a concrete-filled drum with two equal size bubbles of half the original volume. The single bubble is located in the center of the drum, the two smaller bubbles are put in different locations. The mean values at the begining and at the end of the plot are due to the air outside the drum and for steel caps. Inside the drums the mean values for both bubble scenarios give the same results as the concrete, except where the bubbles are. Where the bubbles are, their mean value exceeds the mean for the concrete. The difference is larger for larger bubbles. From the difference, the location of the bubbles can be determined.

The results show that the method presented in section 2.1 allows to determine the total volume of the gas bubbles, while by slicing the drum and repeating the analysis using the same data, a single large bubble can be distinguished from a two bubbles scenario.

Gas bubbles can occur close to uranium blocks. This potentially affects the method as the μ_{discr} for uranium is lower than concrete-like material while the μ_{discr} for gas is higher than for concrete-like. Therefore the presence of the uranium could potentially mask the presence of a gas bubble. This scenario was studied by comparing the results for a 2 litres bubble placed in the middle of the drum with a scenario where a small uranium block was placed next to it. The side of the uranium cube was 3 cm. Figure 12 shows three different geometries: the concrete-filled drum, a 2 litres bubble placed in the center with an uranium cube placed next to it and the 2 litres, single bubble in the center of the drum. The plot shows the lower mean value for the uranium block while

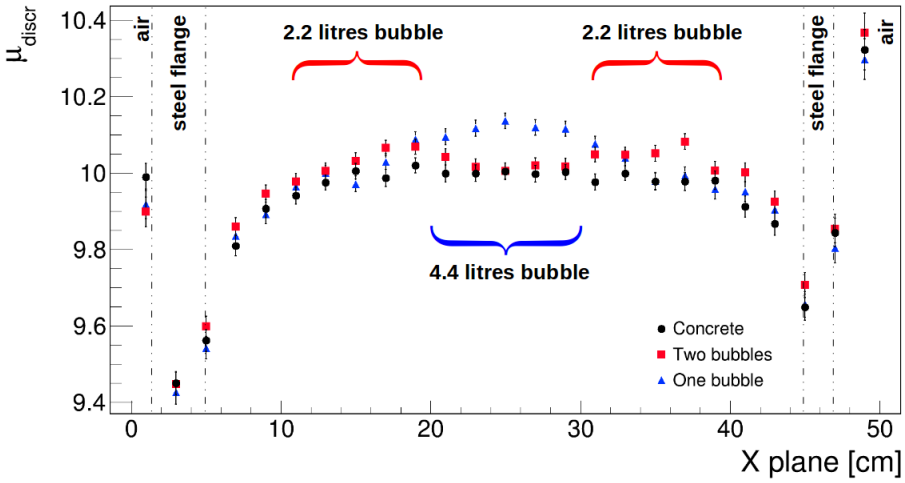

Figure 11: The concrete-filled drum with 4.4 litres bubble inside (blue triangles) or two 2.2 litres bubbles (red squares).

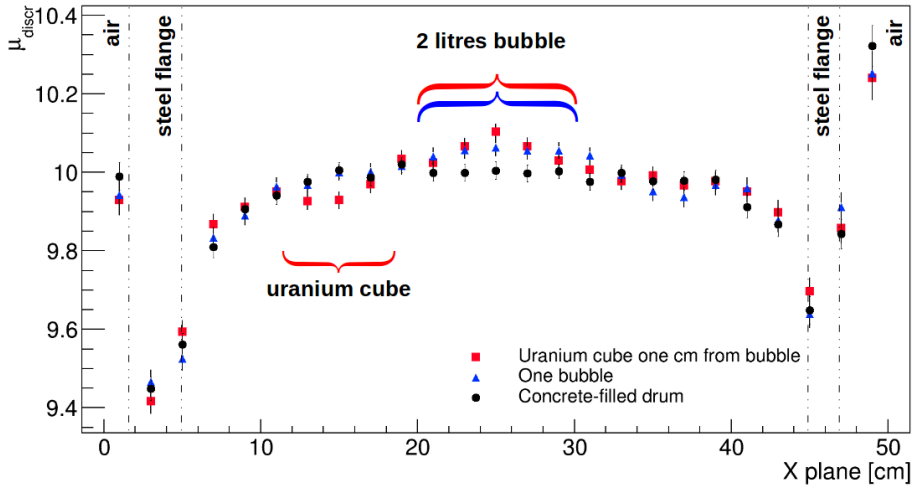

Figure 12: The concrete-filled drum with a 2 litres bubble and an uranium block (red squares) or the concrete-filled drum with a 2 litres bubble (blue triangles).

the higher mean for the adjacent bubbles is also clearly visible. Hence, by applying this method it is also possible to identify the block of uranium with a gas bubble next to it. The uranium cube, put next to gas bubble, does not mask the presence of the gas bubble.

3 Conclusions

In nuclear waste drums hydrogen gas is formed. This is potentially dangerous. Muon Scattering Tomography is a powerful tool to determine the unknown content of a waste drum. We have shown, using Monte Carlo simulations and the proposed method, that it is possible to precisely detect hydrogen bubbles with a volume larger than 2 litres. Using Muon Scattering Tomography it was shown that it is possible to measure the volume of bubbles of two litres or more with a relative

uncertainty resolution of 1.55 ± 0.77%. The results are shown to be independent of the location, shape and distribution of the gas bubbles. By applying this technique to small slices of the volume under tests it is even possible to distinguish a large gas volume from several small ones. Different values for the discriminator are obtained for large bubbles compared to several small bubbles in a given slice, as shown in Figures 10, 11 and 12. Furthermore, we have shown that the proximity of a small piece of high-Z material, here uranium, does not mask the presence of the gas bubble. All this means that the method can be used in real life as it finds bubbles including their location in bituminized waste.

This paper presents a proof-of-concept study, with assumptions that we found reasonable, and the hardware corresponding to the existing prototype build at the University of Bristol. We believe that the detection system can be improved, for example by using larger-area RPCs or applying larger gap between detection planes, which should improve the angular resolution. Thus, the measurement time necessary for achieving a precision required by an industry partner could be reduced. Such numerical and experimental optimization studies will be carried out in the near future.

Acknowledgments

This project has received partial funding from the Euratom research and training programme 2014-2018 under grant agreement No 755371.

References

[1] Dr. Elie Valcke. Experts report on the bituminisation of operational radioactive waste of the Atucha II Nuclear Power Plant, Boeretang 200, 2400 Mol, Belgium, August, 2006.

[2] Michael I Ojovan and William E Lee. *An introduction to nuclear waste immobilisation*. Newnes, 2013.

[3] Morgan P. and Mulder A. *The shell bitumen industrial handbook. Shell Bitumen, ISBN-0-95 16625-1-1*. Thomas Telford, 1995.

[4] JW Frank and AH Roebuck. Crevice corrosion of uranium and uranium alloys. Technical report, Argonne National Lab., Lemont, Ill., 1955.

[5] M McD Baker, LN Less, and S Orman. Uranium+ water reaction. part 1. kinetics, products and mechanism. *Transactions of the Faraday Society*, 62:2513–2524, 1966.

[6] A Danon, JE Koresh, and MH Mintz. Temperature programmed desorption characterization of oxidized uranium surfaces: Relation to some gas uranium reactions. *Langmuir*, 15(18):5913–5920, 1999.

[7] C Thomay, JJ Velthuis, P Baesso, D Cussans, PAW Morris, C Steer, J Burns, S Quillin, and M Stapleton. A binned clustering algorithm to detect high-z material using cosmic muons. *Journal of Instrumentation*, 8(10):P10013, 2013.

[8] C Thomay, J Velthuis, T Poffley, P Baesso, D Cussans, and L Frazão. Passive 3d imaging of nuclear waste containers with muon scattering tomography. *Journal of Instrumentation*, 11(03):P03008, 2016.

[9] C Thomay, JJ Velthuis, P Baesso, D Cussans, C Steer, J Burns, S Quillin, and M Stapleton. A novel markov random field-based clustering algorithm to detect high-z objects with cosmic rays. *IEEE Transactions on Nuclear Science*, 62(4):1837–1848, 2015.

[10] L Frazão, J Velthuis, C Thomay, and C Steer. Discrimination of high-z materials in concrete-filled containers using muon scattering tomography. *Journal of Instrumentation*, 11(07):P07020, 2016.

[11] F Ambrosino, L Bonechi, L Cimmino, R D'Alessandro, DG Ireland, R Kaiser, DF Mahon, N Mori, P Noli, G Saracino, et al. Assessing the feasibility of interrogating nuclear waste storage silos using cosmic-ray muons. *Journal of Instrumentation*, 10(06):T06005, 2015.

[12] A Clarkson et al. Characterising encapsulated nuclear waste using cosmic-ray muon tomography, 2015. *arXiv preprint arXiv:1410.7192*, 10:P03020.

[13] Konstantin Borozdin, Steven Greene, Zarija Lukić, Edward Milner, Haruo Miyadera, Christopher Morris, and John Perry. Cosmic ray radiography of the damaged cores of the fukushima reactors. *Physical review letters*, 109(15):152501, 2012.

[14] Haruo Miyadera, Konstantin N Borozdin, Steve J Greene, Zarija Lukić, Koji Masuda, Edward C Milner, Christopher L Morris, and John O Perry. Imaging fukushima daiichi reactors with muons. *Aip Advances*, 3(5):052133, 2013.

[15] Larry J Schultz, Gary S Blanpied, Konstantin N Borozdin, Andrew M Fraser, Nicolas W Hengartner, Alexei V Klimenko, Christopher L Morris, Chris Orum, and Michael J Sossong. Statistical reconstruction for cosmic ray muon tomography. *IEEE transactions on Image Processing*, 16(8):1985–1993, 2007.

[16] HKM Tanaka, K Nagamine, SN Nakamura, and K Ishida. Radiographic measurements of the internal structure of mt. west iwate with near-horizontal cosmic-ray muons and future developments. *Nuclear*

Instruments and Methods in Physics Research Section A: Accelerators, Spectrometers, Detectors and Associated Equipment, 555(1):164–172, 2005.

[17] G Ambrosi, F Ambrosino, R Battiston, A Bross, S Callier, F Cassese, G Castellini, R Ciaranfi, F Cozzolino, R D'Alessandro, et al. The mu-ray project: Volcano radiography with cosmic-ray muons. *Nuclear Instruments and Methods in Physics Research Section A: Accelerators, Spectrometers, Detectors and Associated Equipment*, 628(1):120–123, 2011.

[18] C Carloganu, V Niess, S Béné, Emmanuel Busato, P Dupieux, F Fehr, Pascal Gay, Didier Miallier, B Vulpescu, Pierre Boivin, et al. Towards a muon radiography of the puy de dôme. *Geoscientific Instrumentation, Methods and Data Systems*, 2:55–60, 2013.

[19] Konstantin N Borozdin, Gary E Hogan, Christopher Morris, William C Priedhorsky, Alexander Saunders, Larry J Schultz, and Margaret E Teasdale. Surveillance: Radiographic imaging with cosmic-ray muons. *Nature*, 422(6929):277–277, 2003.

[20] P Checchia. Review of possible applications of cosmic muon tomography. *Journal of Instrumentation*, 11(12):C12072, 2016.

[21] P Baesso, D Cussans, C Thomay, and J Velthuis. Toward a rpc-based muon tomography system for cargo containers. *Journal of Instrumentation*, 9(10):C10041, 2014.

[22] PARTICLE DATA GROUP collaboration, J. Beringer et al.,. Review of particle physics. *Phys. Rev. D*, 86:010001, Jul 2012.

[23] D Reyna. A simple parameterization of the cosmic–ray muon momentum spectra at the surface as a function of zenith angle. *arXiv preprint hep-ph/0604145*, 2006.

[24] Simon Eidelman, KG Hayes, KA ea Olive, M Aguilar-Benitez, C Amsler, D Asner, KS Babu, RM Barnett, J Beringer, PR Burchat, et al. Review of particle physics. *Physics Letters B*, 592(1), 2004.

[25] Marcia Flavia Righi Guzella and TV Silva. Evaluation of bitumens for radioactive waste immobilization. *Waste Management*, 2001.

[26] P Baesso, D Cussans, C Thomay, JJ Velthuis, J Burns, C Steer, and S Quillin. A high resolution resistive plate chamber tracking system developed for cosmic ray muon tomography. *Journal of Instrumentation*, 8(08):P08006, 2013.

[27] Chris Hagmann, David Lange, and Douglas Wright. Cosmic ray shower generator (cry) for monte carlo transport codes. In *Nuclear Science Symposium Conference Record, 2007. NSS'07. IEEE*, volume 2, pages 1143–1146. IEEE, 2007.

[28] Sea Agostinelli, John Allison, K al Amako, J Apostolakis, H Araujo, P Arce, M Asai, D Axen, S Banerjee, G Barrand, et al. Geant4 a simulation toolkit. *Nuclear instruments and methods in physics research section A: Accelerators, Spectrometers, Detectors and Associated Equipment*, 506(3):250–303, 2003.